Thermodynamic and Hydrogen-Bonding Analyses of the Interaction between Model Lipid Bilayers

Changsun Eun and Max L. Berkowitz*

Department of Chemistry, University of North Carolina at Chapel Hill, Chapel Hill, North Carolina 27599

Received: October 29, 2009; Revised Manuscript Received: January 14, 2010

This paper presents further analysis of a system containing two graphene plates with attached phosphatidylcholine lipid headgroups embedded in water, which models a lipid bilayer. Previously, we performed molecular dynamics simulations on this system, calculated the potential of mean force (PMF) between plates (Eun, C.; Berkowitz, M. L. *J. Phys. Chem. B* **2009**, *113*, 13222−13228), and also performed a structural analysis of water in the confined space between the plates. Here, we perform thermodynamic analysis of the PMF and, in addition to the previous analysis of water that considered density plots and the OH bond orientational profiles, we perform hydrogen bonding analysis of water. We show that the structural analysis of water is consistent with the thermodynamic results we obtained for the PMF.

I. Introduction

The hydration force acting between neutral lipid bilayers was first measured by Lenevue et al. in 1976.[1] While initially it was assumed that the force is exponentially decaying over the whole distance interval, more detailed measurements[2] showed that the force of interaction between neutral lipid bilayers in the liquid crystalline phase has three regimes: a long-range regime when the fluid spacing between membranes exceeds ∼1 nm due to bilayer undulations, a short-range regime (when fluid spacing is below ∼0.4 nm) due to steric repulsion of bilayers, and, finally, the intermediate-range regime, which is actually due to water and represents the proper "hydration" force. In addition to experimental work, a large amount of theoretical and simulation work[3−16] has been done to explain the nature of the hydration force. Recently, we performed molecular dynamics simulations on a model system, where the neutral lipid bilayer was represented as a graphene plate with attached phosphatidylcholine (PC) lipid headgroups, which we called PC-headgroup plates.[17] We used a model system to be able to efficiently calculate the free energy (or the potential of mean force, PMF) of plate interaction as a function of distance between plates and also to determine general principles related to the structure of water that induces the hydration force.

Lately, a lot of attention has been devoted to understanding the nature of interaction between hydrophobic particles.[18−20] To study characteristics of a possible hydrophobic interaction between nanoscale particles, Choudhury and Pettitt performed simulations on a system containing two graphene plates immersed in water.[21−23] To study the interaction between model hydrophilic particles, Lu and Berkowitz[15,24] used the graphene plates from the Choudhury and Pettitt simulations and assigned charges to certain carbon atoms, so that the plates, while being neutral, had charges distributed on them. To connect their study to the problem of the hydration force acting between lipid bilayers, Lu and Berkowitz assigned charges in such a way that the charges, in a coarse-grained fashion, represented the zwitterionic character of lipid bilayers, such as dipalmitoylphosphatidylcholine (DPPC). The major shortcoming of the model used by Lu and Berkowitz was the rigid character of the dipoles. In our previous work,[17] we again studied the interaction between model hydrophilic surfaces, though, this time, the headgroups of lipids were faithfully represented and were allowed to move. Thus, our system contained two graphene plates (2.425 nm × 2.380 nm) with nine phosphatidylcholine (PC) headgroups attached to these plates, so that the area per headgroup is 0.64 nm^2, a value typical of the PC area observed in lipid bilayer experiments[25] and computer simulations.[26,27] The two plates separated by a certain distance were immersed into a large simulation box containing 8800 SPC/E water[28] molecules. The schematic picture of the system simulated, including a more detailed representation of the hydrophilic model plates and of the headgroup, is given in Figure 1.

Our previous calculations showed that the PMF has a repulsive character over all interplate distances. We also determined that the PMF has three regimes, and we were able to fit each of these to an exponential function. In parallel to the total PMF calculation, we also calculated the contributions to the free energy change due to the direct interaction between the plates and the water-mediated interaction. The total PMF, the direct contribution, and the water-mediated contribution are shown in Figure 2. We determined that the small distance regime of the interaction, when the plates are at distances below 1 nm and the fluid spacing below 0.1 nm, is due to steric repulsion between the headgroups. The intermediate distance regime, when the interplate distance is between 1 and 1.6 nm and the fluid spacing between 0.1 and 0.7 nm, is due to the removal of water structured by the surfaces. Finally, the large distance regime was also determined to be due to water in our simulation. In both the intermediate and large distance regimes, the water-mediated contribution acts in opposition to the direct contribution while the water-mediated contribution dominates. While both the water-mediated and direct contributions are small and nearly cancel in the large distance regime, the inset of Figure 2 with displayed error demonstrates that the total PMF in the large distance regime is due to water, which indicates that water is still slightly disturbed when the distance between the plates is in the range 1.6 to ∼2.2 nm with a fluid spacing of 0.7 to ∼1.3 nm. Since the long-range membrane undulation modes were not present in our simulations due to computational restrictions, our PMF could not have an undula-

* To whom correspondence should be addressed. E-mail: maxb@unc.edu.

10.1021/jp910347n
Published on Web 02/10/2010

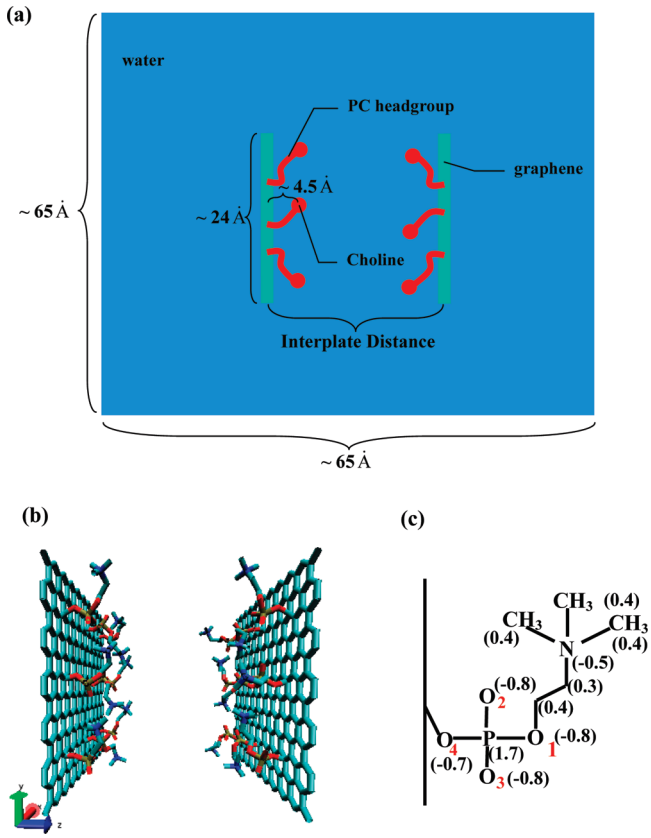

Figure 1. (a) Schematic diagram of our model system with associated length scales. (b) Snapshot of the PC-headgroup plates. (c) Detailed structure of the PC headgroup. The numbers in parentheses represent the magnitudes of partial charges (in units of the elementary charge, *e*).

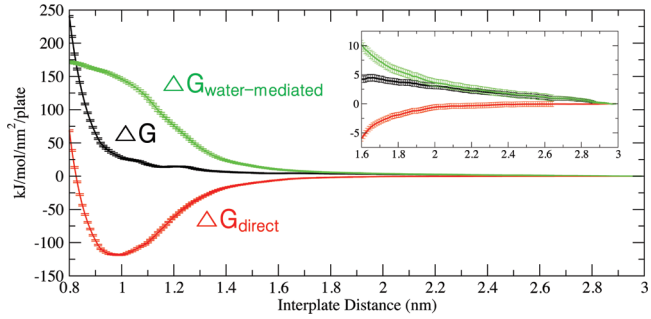

Figure 2. Decomposition of the PMF (black) into contributions from the direct interaction (red) and from the water-mediated interaction (green). Inset is for large interplate distances. Errors are represented by bars.

tion contribution. We also studied water properties by analyzing density profiles and orientational distributions of OH bonds of water in the confined region and showed that structure of water is connected to the length scales of the three regimes observed in the PMF.

In this work, we further pursue our study of the nature of the PMF acting between lipid bilayers by performing a thermodynamic analysis of this PMF. We also perform an analysis of the hydrogen bonding network for water in confined space and show that this analysis may explain why water contributes to the PMF in the long-range regime. Our present work should be considered as complementary to our previous work that used the same model.

II. System and Computational Details

The same arrangement of the system as described in our previous paper[17] is used in this work, with a depiction of the system provided in Figure 1. Previously we calculated the potential of mean force (PMF) between the two plates at thermodynamic conditions of $P = 1$ bar and $T = 298$ K. For this purpose, we performed molecular dynamics (MD) simulations on the system with plates fixed at a set of different interplate distances and used thermodynamic perturbation method[23] to obtain the PMF curve. The interplate distance was defined by the distance between two graphene plates. During the simulations the box size fluctuated around values of 6.5 nm × 6.5 nm × 6.5 nm. For our NPT simulations we used Nose−Hoover[29,30] temperature coupling and Parrinello−Rahman[31] pressure coupling algorithms. Electrostatic interaction was calculated through the particle mesh Ewald method.[32] More details about the preparation of the system and molecular dynamics simulations were described in the previous paper.[17]

To separate the PMF into the enthalpy−entropy contributions, we used the thermodynamic definition of entropy and employed the finite difference method[22,33] for its calculation:

$$-\Delta S(r) \equiv \left(\frac{\partial \Delta G(r)}{\partial T}\right)_{N,P} \cong \left(\frac{\Delta G(r, T + \mathrm{d}T) - \Delta G(r, T)}{\mathrm{d}T}\right)_{N,P} \quad (1)$$

where $\Delta S(r)$ and $\Delta G(r)$ are the entropy and the Gibbs free energy changes from the reference state ($r = 2.99$ nm, where the free energy was assumed to have a zero value), to the state when the interplate distance had a value of r. In our calculation, the temperature difference, dT, was 10 K, thus requiring us to carry out an additional simulation at 308 K. Once we determined the entropy change, we calculated the enthalpy change, $\Delta H(r)$, by using the equation

$$\Delta H(r) = \Delta G(r) + T\Delta S(r) \quad (2)$$

Since PMF can be decomposed into contributions originating from the direct interaction between plates and water-mediated interaction,[17] as shown by eq 3:

$$\Delta G(r) = \Delta G_{\mathrm{direct}}(r) + \Delta G_{\mathrm{water\text{-}mediated}}(r) \quad (3)$$

we applied the finite difference method to each type of interaction and calculated enthalpic and entropic contributions for both direct and water-mediated interactions as well. In addition, to obtain a better understanding for the details involved in the enthalpy change, we calculated the potential energy change with respect to the reference state ($\Delta U(r)$), directly from the MD simulation at each interplate distance r, and further decomposed $\Delta U(r)$ into multiple terms:

$$\Delta U(r) = \Delta U_{\mathrm{direct}}(r) + \Delta U_{\mathrm{water\text{-}mediated}}(r) = \Delta U_{\mathrm{direct}}(r) + \Delta U_{\mathrm{water-water}}(r) + \Delta U_{\mathrm{PC\ plate-water}}(r) \quad (4)$$

where $\Delta U_{\mathrm{direct}}(r)$ and $\Delta U_{\mathrm{water\text{-}mediated}}(r)$ are, respectively, the interaction potential energy between the PC-headgroup plates and the potential energy involving water molecules, which can be further separated into a water−water interaction ($\Delta U_{\mathrm{water-water}}(r)$) and a water−plate interaction ($\Delta U_{\mathrm{PCplate-water}}(r)$). All terms except $\Delta U_{\mathrm{PCplate-water}}(r)$ are

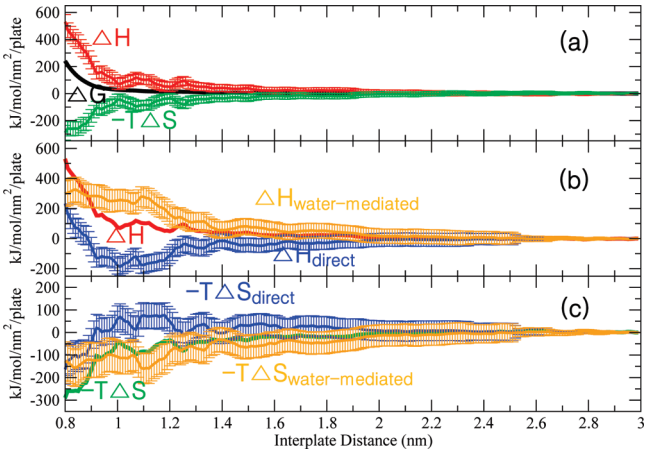

Figure 3. (a) Enthalpic (red) and entropic (green) contributions to the PMF (black). (b) Decomposition of the enthalpic contribution (red) into the direct interaction (blue) and the water-mediated interaction (orange). (c) Decomposition of the entropic contribution (green) into the direct interaction (blue) and the water-mediated interaction (orange). Errors are represented by bars.

computed directly from the simulations, and $\Delta U_{\mathrm{PCplate-water}}(r)$ is determined from eq 4.

Analysis of the hydrogen bonding network is a key ingredient for understanding the water−water and water−plate interactions. Therefore, we performed hydrogen bonding analysis using the standard geometry criterion for hydrogen bonds (H-bonds). According to this criterion, when the distance between oxygen atoms of the H-bond donor and the H-bond acceptor ($|\overrightarrow{OO}|$) is less than 0.35 nm and the angle between $|\overrightarrow{OH}|$ of the H-bond donor and $|\overrightarrow{OO}|$ is less than 30° and the hydrogen−oxygen (H-bonded) distance is less than 0.245 nm, a hydrogen bond is considered to be formed.[34] Based on this criterion, we calculated the profiles of the number of H-bonds per water molecule and the number of H-bond donors/acceptors per water molecule. In that calculation, the position of the oxygen atom in a water molecule is considered as the position of the water molecule.

Errors for the PMF and the enthalpy−entropy calculation were estimated by using the block averaging method[35] and the standard error propagation method. For potential energy calculations and hydrogen bond calculations, we simply considered the standard deviation as an error.

All MD simulations were performed using the GROMACS 3.3.1[36] and GROMACS 3.3.3[36] suite of programs.

III. Results and Discussion

III.1. Thermodynamics. ***Enthalpic and Entropic Contributions.*** To understand the thermodynamic basis behind the repulsive character of the interaction between our two hydrophilic plates immersed in water, we carried out entropy−enthalpy analysis of the PMF curve through the use of eq 1. The result is shown in Figure 3a. As we can see from this figure, while the enthalpic contribution is unfavorable when we squeeze the water out from the space between the plates, the entropic contribution is favorable (note that we plot the negative of the entropy change in units of energy ($-T\Delta S(r)$)).

For a more detailed understanding of the enthalpic and entropic parts of the PMF, we separated the entropic and enthalpic contributions further into direct and water-mediated contributions as depicted in Figure 3b,c. Figure 3b illustrates that the enthalpy change is dominated by the water-mediated contribution that is unfavorable due to removal of water from the interplate space. The direct contribution to the enthalpy change is favorable for large and intermediate distances and unfavorable for small distances; in its shape it is reminiscent of a van der Waals interaction as can be expected. The behavior of the direct and the water-mediated components contributing to the entropic part of the free energy change is shown in Figure 3c. As the figure shows, due to the release of water into the bulk-like environment, the water-mediated contribution is favorable at both intermediate and small distances. The direct contribution to entropy change is unfavorable at intermediate distances, but it is favorable at small. This likely is happening because, at intermediate distances, water restricts the conformational motion of the headgroups to support its hydrogen bonding network. Release of water, when the distance between plates decreases, removes the conformational constraints on these headgroups; as a result, the entropy increases. It is very hard to judge what is happening in the large distance regime (at distances above 1.6 nm), since the error bars on Figure 3c are large in this regime.

Overall, the results displayed in Figures 2 and 3 show that the enthalpy change dominates the repulsive nature of the PMF. The results also show that the water-mediated contribution determines the repulsive nature of the PMF in the intermediate regime and that the water-mediated contribution is dominant for both entropy and enthalpy changes in this regime.

Potential Energy Change. Why is the water-mediated contribution into enthalpy change positive as the distance between plates decreases? To address this question, we need to perform a more detailed investigation of $\Delta H(r)$. Since enthalpy has two components (internal energy and a PV-work term, where P and V are pressure and volume of the system), we need to consider the internal energy change ($\Delta E(r)$) and the PV change (ΔPV) with respect to the reference state. The internal energy change can be directly calculated from the simulations. Regarding the PV term, it can be determined either by subtracting $\Delta E(r)$ from $\Delta H(r)$ or by direct calculation from the simulation. Since our simulations were done at constant P, and since we observed that the volume change is very small, the ΔPV term can be neglected. Furthermore, since the temperature of the system is constant, the kinetic energy change is zero and, thus, the internal energy change is equal to the potential energy change. In summary, $\Delta H(r) \approx \Delta E(r) \approx \Delta U(r)$. Therefore, the enthalpy change can be numerically calculated either from a difference between the free energy change and entropy change or directly from the energy change; in fact, Zangi and Berne[37] used the latter method to calculate $\Delta H(r)$. Because our calculations contain numerical noise the results for enthalpy change from the two methods are not identical, but are still quite similar. Therefore, to examine the details of the enthalpy change, we examined the details of the potential energy change.

The total potential energy can be considered to be a sum of two terms: the first term due to the potential energy of interaction between two PC-headgroup plates ($\Delta U_{\mathrm{direct}}$) and the second term involving water molecules ($\Delta U_{\mathrm{water\text{-}mediated}}$). For more detailed analysis, we also performed a separation of $\Delta U_{\mathrm{water\text{-}mediated}}$ into contributions from $\Delta U_{\mathrm{PCplate-water}}$ and $\Delta U_{\mathrm{water-water}}$ according to eq 4; these are depicted in Figure 4. We observed that, as the interplate distance decreases, $\Delta U_{\mathrm{PCplate-water}}$ begins to increase at ∼1.6 nm and is saturated ∼1 nm, whereas $\Delta U_{\mathrm{water-water}}$ decreases until the interplate distance is ∼1 nm and then increases. The increase of $\Delta U_{\mathrm{PCplate-water}}$ with the decrease of the distance in the intermediate regime, especially in the distance interval from ∼1.6 to ∼1.3 nm, is somewhat unexpected as the number of hydrogen bonds between water and plates is not

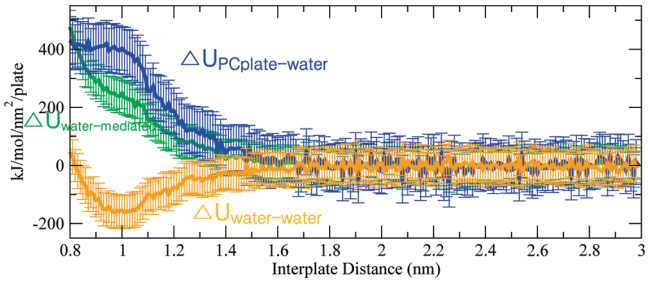

Figure 4. Potential energy contribution involving water molecules (green), further decomposed into the following two terms: potential energy of interaction between the PC-headgroup plates and water (blue) and potential energy of interaction between water molecules (orange). Error bars are obtained from standard deviation.

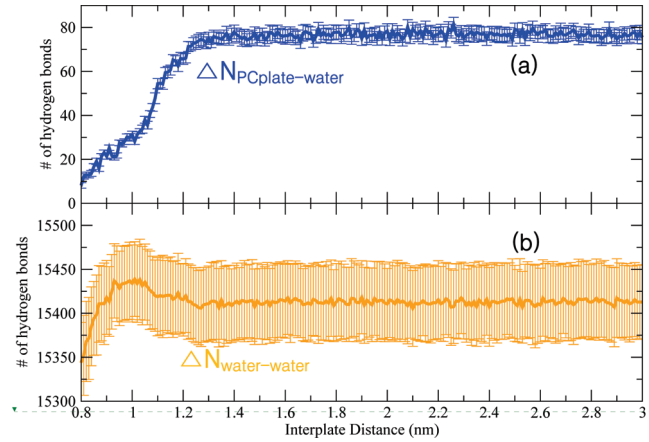

Figure 5. (a) Average number of hydrogen bonds between the PC-headgroup plates and water as a function of interplate distance. (b) Average number of hydrogen bonds between water molecules as a function of interplate distance. For direct comparison with Figure 3 we used the same colors. Error bars are obtained from standard deviation.

expected to change in this regime (see below). This increase, therefore, must be due to the decrease in the number of water molecules that interact with the PC-headgroups, but not through hydrogen bonding.

The observed behavior for the $\Delta U_{\text{water}-\text{water}}$ is not difficult to explain. At the intermediate separations, when the confined water molecules leave the interplate space for the bulk, the potential energy for water−water interaction decreases because the escaped water molecules interact with more water molecules in the bulk-like environment. At small separations, the water−water potential energy increases, as some water molecules (especially, waters next to phosphate groups) stay in the confined space due to a strong interaction between water and the plate, and these water molecules are more and more isolated from the water network as the interplate distance decreases.

From our analysis, we therefore conclude that in the intermediate distance regime the increase in energy of water−plate interaction dominates over the decrease in water−water interaction energy: this balance is responsible for the observed positive change in the water-mediated contribution into the enthalpy as the distance between plates diminishes in the intermediate distance regime.

III.2. Hydrogen Bonding Analysis. In our previous work[17] we demonstrated that three different groups of water molecules exist in the confined space between PC-headgroup plates. The first group contains water molecules that are hydrogen bonded to phosphate groups of lipid headgroups and located in close proximity to phosphates; thus these molecules were named accordingly as phosphate waters. The second group contains water molecules around choline groups of the headgroups, i.e., molecules at the headgroup/water interface, and therefore these water molecules are named interfacial waters. Finally, the rest of the water molecules situated further from the surfaces were named bulk-like waters, although, as we will see, not all of them display bulk-like properties. We connected the different interaction regimes to changes in the water structure and the amount of water in the different groups mentioned above. It is clear that the thermodynamic changes we discussed in section III.1 are also associated with the change of the hydrogen bonding network. Below, we present an analysis of changes in the water hydrogen bonding network as the distance between plates changes, and we also present the connection between these changes and the thermodynamics of the system.

Number of Hydrogen Bonds. Based on the criteria presented in section II, we calculated the average numbers of hydrogen bonds between the plates and water molecules, and between water molecules themselves as functions of interplate distance. Note that this calculation was performed for the entire space, and not only for the confined space, because the thermodynamic changes discussed in section III.1 result from changes which occurred in and out of the confined space. The results are reported in Figure 5. As we can see, the behavior of an average number of hydrogen bonds formed between plates and water in Figure 5a and the number of water−water hydrogen bonds from Figure 5b is consistent with the behavior of water-mediated potential energy change from Figure 4. Indeed, in the interval 1.6−1.3 nm, the number of water−plate hydrogen bonds does not change; therefore, the increase in water−plate interaction energy in this interval is due to non-hydrogen bonding energy change. The number of water−plate hydrogen bonds starts diminishing when the distance gets below 1.3 nm, and consequently, the water−plate interaction energy increases due to the loss of water−plate hydrogen bonding. The number of water−water hydrogen bonds also does not change before the distance between plates reaches 1.3 nm; it is the change in the strength of hydrogen bonding that decreases the energy of water−water interaction when the distance between plates is above 1.3 nm. Below the distance of 1.3 nm, the number of water−water bonds increases, and therefore, the corresponding energy decreases. When the interplate distance becomes smaller than 1 nm, the number of water−water hydrogen bonds decreases and the energy correspondingly increases.

As we observed from Figure 5a, the decrease in the number of hydrogen bonds begins at ∼1.3 nm. This implies that some of the interfacial water molecules can also make hydrogen bonds with the phosphate groups of the plates, as phosphate waters do. Moreover, the fact that the strength of hydrogen bond between phosphates of the plate and water molecules is stronger than that between water molecules[38] can explain why the contribution of $\Delta U_{\text{PCplate}-\text{water}}$ into $\Delta U_{\text{water-mediated}}$ at distances below 1.3 nm is larger than the contribution of $\Delta U_{\text{water}-\text{water}}$. This shows that the presence of PC headgroups strongly influences the structure of the water network; similar perturbation by polar headgroups to the water hydrogen bond network is also observed in solutions containing micelles[39] and reverse micelles.[40,41]

Hydrogen Bond Density Profiles. In our previous work[17] we performed density and orientational analyses of water between the PC-headgroup plates. We observed that water has bulk-like properties in the middle of the interplate space when the distance between plates is above 1.6 nm. At the same time, we observed that the repulsive interaction is present at the distances beyond

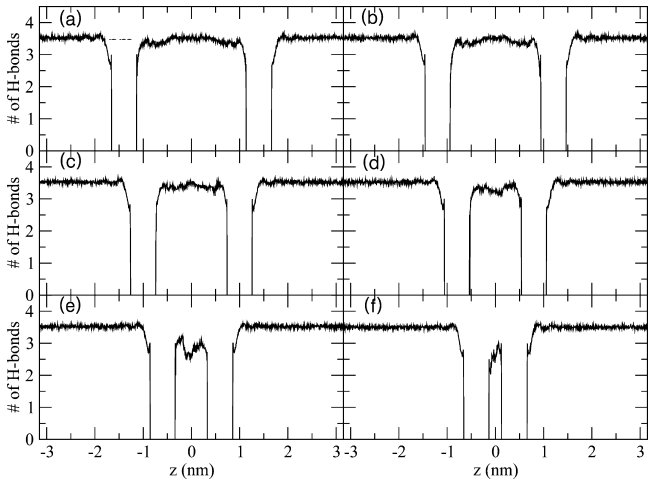

Figure 6. Profiles of the number of hydrogen bonds per water molecule at the interplate distances of 2.8 (a), 2.4 (b), 2.0 (c), 1.6 (d), 1.2 (e), and 0.8 nm (f).

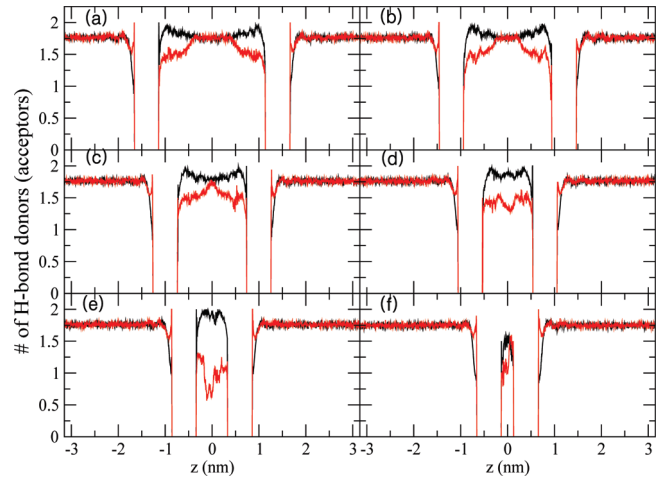

Figure 7. Profiles of the numbers of hydrogen bond donors (black) and acceptors (red) per water molecule at the interplate distances of 2.8 (a), 2.4 (b), 2.0 (c), 1.6 (d), 1.2 (e), and 0.8 nm (f).

1.6 nm and it is also due to water. To understand the properties of water in the confined space between the plates and in the hope to observe that confined water is different from bulk water even when the interplate distance is beyond 1.6 nm, we calculated the average number of hydrogen bonds per water molecule in the confined space. In this calculation, all hydrogen bonds were taken into account, irrespective of whether the bonds were made with the PC headgroups or with other water molecules. The results are displayed in Figure 6. Here, the abscissa depicts the z axis of the system, which is perpendicular to both plates. The z coordinate of the point at the center between the two plates is set to zero and serves as a reference point. Thus, for example, if the two plates are at an interplate distance of 2.0 nm, one plate is situated at −1.0 nm and the other is at 1.0 nm. For comparison with the bulk water, water outside the plates (but confined in the xy dimensions to the plate size) is also considered.

Figure 6 indicates that the average number of hydrogen bonds per water molecule in the bulk (outside the confined space) is around 3.5, which is consistent with the previous calculation by Choudhury and Pettitt.[23] However, the number of hydrogen bonds per water molecule in the confined space is generally less than 3.5, especially at the intermediate and small separations (Figure 6d−f). We observed that the closer the plates are and the more confined the water is, the more the structure of water deviates from the bulk-like arrangement with its characteristic ∼3.5 hydrogen bonds per water molecule. We can also compare the shapes of the profiles in the interplate space obtained in this work with profiles obtained for the case of hydrophobic plates.[23] Although in both cases the heights of the profiles in the confined region decrease as the interplate distance decreases, in our case the decreasing height displays an undulating character, absent in the hydrophobic case. Clearly, in our case, as in the hydrophobic case, the confined water is restructured, but the water structure itself is different from the structure present in the hydrophobic case due to the different boundary conditions provided by hydrophilic and hydrophobic plates, respectively.

To better understand the details of the hydrogen bonding network in the confined water, we performed an additional analysis by specifying the donor or acceptor character of the hydrogen bond, i.e., by decomposing the number of hydrogen bonds per water molecule into two components: number of donor bonds and number of acceptor bonds. These numbers are equal for bulk water, but in the confined space between the plates, due to a specific structure of the network, we cannot expect them to be equal. Moreover, we expect the numbers to depend on the position along the z axis between the plates. Indeed, since our PC-headgroup plates have H-bond acceptors due to phosphates, water molecules next to the plates are mostly H-bond donors. However, for the confined water molecules that are situated further away, the opportunity to make hydrogen bonds with the phosphates decreases and, therefore, we expect the number of H-bond donors to decrease, while the number of H-bond acceptors per water molecule increases. This is indeed the situation, as one can see from Figure 7.

Interestingly, the plots from Figure 7 allow us to perform a comparison of the H-bond donor/acceptor character of water molecules next to either hydrophobic or hydrophilic plates, since our PC-headgroup plate has both hydrophobic (outward with respect to the confined space) and hydrophilic (inward) sides. Both sides have a common feature in that they disturb the adjacent water structure, but in a very different way. The disparity in acceptor/donor character for water next to the hydrophobic side is short ranged (∼0.25 nm), while the hydrophilic side has a longer range (∼0.8 nm). From Figure 7 we observed that, next to the hydrophobic side, the average number of H-bond acceptors per water molecule is larger than the average number of H-bond donors. This occurs because, as it was observed previously, one of the OH bonds of the water molecule has a tendency to point toward the hydrophobic surface,[42] therefore diminishing its possibility to engage in hydrogen bonding as a H-bond donor. Contrary to this effect, near the hydrophilic side of the plate (the side with the PC headgroups), the average number of H-bond donors per water molecule is larger than the average number of H-bond acceptors, because, as was already explained above, of the presence of phosphate groups that accept hydrogen bonds from water. As we observed in our previous work, phosphate waters are nearly parallel to the plates and, therefore, can donate both of their hydrogen bonds to the plates; this is why the shoulders of hydrogen bond donor curves in Figure 7a−c reach the value of ∼2.

The hydrogen bonding density plots presented in Figure 7 from this paper are complementary to the number density and the orientational profile plots from our previous work.[17] Together, the plots provide a qualitative description of the water structure in the interplate space. At large separations, such as the ones depicted in Figure 7a,b, real bulk-like water is present

in the middle of the confined region. However, when the distance between plates is reduced below 2.1 nm (Figure 7c), the discrepancy in the number of donors and acceptors per water molecules appears, indicating that water starts deviating from having truly bulk-like characteristics. Note that both density profiles and orientational properties of water from our previous work showed visible deviation from bulk-like properties only when the distance between plates was below 1.6 nm. The deviation of water from having true bulk properties at distances above 1.6 nm that hydrogen bonding profiles in Figure 7 display is consistent with our observation of the large distance regime in the PMF. When the interplate distance is further reduced to 1.6 nm (see Figure 7d) and the intermediate distance regime of the PMF begins, the water molecules in the confined space are strongly perturbed, as the OH bond orientation and density profiles of water,[17] as well as hydrogen bonding profiles, show. The hydrogen bonding profile in Figure 7d is quite distinct from the profile of Figure 7c in that the average number of H-bond acceptors per water molecule is significantly reduced, while the number for H-bond donors per water molecule is slightly increased. Moreover, in the case when an interplate distance has a value of 1.2 nm, which also belongs to the intermediate regime, further reduction in the number of H-bond acceptors takes place, as shown in Figure 7e. This behavior can be understood by referring to the results obtained in our previous work by performing analyses of OH bond orientation of the confined water and investigating the snapshots displaying the hydrogen bonding network (see Figures 6 and 7 in our previous paper[17]). The large reduction in the number of H-bond acceptors and the increase in the number of donors for water molecules in the middle of the confined space are due to the spatial arrangement of waters that serve as "bridging" molecules between phosphates from opposing plates. As the distance between plates is further reduced and the small distance regime is reached (see Figure 7f), all interfacial water molecules are expelled from the confined space. In this case, the hydrogen bonds between phosphates and phosphate water molecules become unstable, and as a result, some OH bonds tend to orient perpendicular to the plates (Figures 6d and 7d in our previous paper[17]). Therefore, at the small distance regime, some of the hydrogen bonds between the phosphate water molecules and phosphates are broken, and the relative difference between the numbers of H-bond acceptors and donors per water molecule is reduced, compared to the cases depicted in Figure 7d or 7e. However, the number of H-bond donors is still large because phosphate groups from the opposing plates play also the role of a H-bond acceptor.

PC Headgroups and Hydrogen Bonding. We also studied in some detail the role of the phosphate of the PC headgroups in the hydrogen bonding network. To determine which oxygen atoms (H-bond acceptors) of the phosphate moiety are contributing the most to the hydrogen bonding network, we calculated the contribution of each of the four oxygen atoms in the moiety to the formation of hydrogen bonds with water molecules. The results are summarized in Table 1. We assigned them numbers from 1 to 4 according to their positions in the backbone, which results in the equivalency of oxygen atoms 2 and 3 (see Figure 1c). Table 1 shows that oxygen atoms 2 and 3 of the phosphate contribute the most (∼80%) to hydrogen bonding, while the contribution of oxygen atom 1 is small (∼20%) and the contribution of the oxygen atom 4 is negligible. This is consistent with our previous observation that the phosphate water molecules are positioned between phosphate groups and make hydrogen bonds with the two oxygen atoms of the group (Figure 7 of our previous paper[17]).

TABLE 1: Contribution (in Percentage) of Each Oxygen Atom of the Phosphates That Are Involved in the Hydrogen Bonding Network as a Function of Interplate Distance

interplate distance (nm)	oxygen atom 1	oxygen atoms 2 and 3	oxygen atom 4
2.8	18.8 (±3.0)	80.8 (±4.8)	0.4 (±0.7)
2.4	19.9 (±2.7)	79.5 (±4.8)	0.6 (±0.8)
2.0	19.2 (±2.7)	80.5 (±4.9)	0.3 (±0.7)
1.6	19.1(±3.0)	80.6 (±5.4)	0.3 (±0.7)
1.2	13.1 (±2.7)	86.5 (±4.6)	0.4 (±0.7)
0.8	16.6 (±9.4)	83.4 (±16.4)	0

IV. Summary and Conclusions

In summary, to explore the interaction between two zwitterionic lipid bilayers, we modeled the bilayers as graphene plates decorated with phosphatidylcholine lipid headgroups and calculated the PMF for the interplate interaction. As we showed in the previous work, this simple model can qualitatively reproduce the interaction between lipid bilayers. In this work, using MD simulations, we calculated the enthalpic and entropic contributions to the PMF. Our result demonstrated that the enthalpic contribution ($\Delta H(r)$) to the PMF is dominant over the entropic contribution ($-T\Delta S(r)$). Perhaps one of the key results from the thermodynamic analysis performed in this work is that the repulsive interaction in the intermediate regime, which is associated with the proper "hydration" force, is due to the loss of water involved in energetically favorable water−surface interaction. We also performed a hydrogen bonding analysis of water in the confined space between our surfaces. This analysis was complementary to our previous analysis, wherein we studied the orientational and density profiles of water in the confined space. The present analysis produced results consistent with the previously reported results on the structure of water between plates. In general, the results from three different types of analysis involving water density plots, OH bond orientational plots, and hydrogen bonding profiles were consistent with our calculated thermodynamic results. Our detailed hydrogen bond analysis also revealed that water is still slightly perturbed when the interplate distance is beyond 1.6 nm. This explains why we observed a long-range regime in the PMF due to water, although it is important to mention here that, in experiments, this regime will be dominated by the undulation force.

Our previous results, together with the results of this paper, show that during the three regimes present in the PMF different types of water are removed from the space between the plates. When the plates approach each other in the long-range regime, we remove the "bulk-like" water, but, as we showed in this work not all of this water is really bulk-like. In the midrange regime, or the proper "hydration force" regime, the water organized by the surfaces is removed. Finally, when we reach the small-range regime, the headgroups crash into each other and dominate the interaction, forcing some of the remaining water in the headgroups to be expelled. Although water most directly influences the interaction in the midrange regime, it also influences the interaction in other regimes through its influence on the headgroup configurations.

The initial theoretical treatment of the hydration force performed by Marcelja and Radic (MR)[3] had a phenomenological character and predicted an exponential decay for the order parameter. While the original paper by MR did not specify the microscopic origin of the order parameter, it was presumed that

the order parameter was likely the orientational polarization of water. We calculated the two types of orientational polarization profiles for water, $\langle \cos \theta(z) \rangle$ and $\langle \cos \theta(z) \rangle n(z)$, where $n(z)$ is the normalized (to bulk value) local density of water along the axis perpendicular to the plates. For the large interplate regime, both profiles could be fitted to the functional form predicted by the MR theory, but the fitting exponents were way out of the range observed in the decay of the PMF. For the intermediate regime, the polarization profiles displayed oscillations and the fit was poor. Moreover, the exponent of the fit also was not in agreement with the one from the PMF. We conclude that the MR theory with orientational polarization as an order parameter cannot explain the behavior of the interaction between our plates. The conclusion that orientational polarization cannot explain the interaction between zwitterionic lipid bilayers has already been obtained previously, based on the results from earlier simulations[11,43] and also on theoretical analysis.[9] Our present calculations just confirm it.

As we already mentioned, the main cause of the repulsive interaction between two bilayers in the intermediate distance regime (or proper hydration force regime) is due to reduction in the favorable interactions between the plate and water molecules, especially due to breaking strong hydrogen bonds between phosphates and water molecules. This suggests that the ability of the phosphate moiety of PC headgroups to make hydrogen bonds with water molecules is very crucial to generating the repulsive interaction between two bilayers. Thus, besides removing water, we expect that a decrease in the polarity of the phosphate moiety can also reduce the repulsive interaction in the hydration force regime. For this reason, and considering the importance of understanding of the role of electrostatic interaction, the direct comparison between the current system and the charge-removed system is very interesting. This investigation is now underway.

Acknowledgment. This work was supported by the National Science Foundation under Grants MCB-0615469 and MCB-0950280. The authors would like to thank Charles Davis for careful reading of the manuscript and useful suggestions.

References and Notes

(1) Leneveu, D. M.; Rand, R. P.; Parsegian, V. A. *Nature* **1976**, *259*, 601.
(2) McIntosh, T. J.; Simon, S. A. *Annu. Rev. Biophys. Biomol. Struct.* **1994**, *23*, 27.
(3) Marcelja, S.; Radic, N. *Chem. Phys. Lett.* **1976**, *42*, 129.
(4) Schiby, D.; Ruckenstein, E. *Chem. Phys. Lett.* **1983**, *95*, 435.
(5) Rand, R. P.; Parsegian, V. A. *Biochim. Biophys. Acta* **1989**, *988*, 351.
(6) Kornyshev, A. A.; Leikin, S. *Phys. Rev. A* **1989**, *40*, 6431.
(7) Leikin, S.; Kornyshev, A. A. *J. Chem. Phys.* **1990**, *92*, 6890.
(8) Leikin, S.; Parsegian, V. A.; Rau, D. C.; Rand, R. P. *Annu. Rev. Phys. Chem.* **1993**, *44*, 369.
(9) Besseling, N. A. M. *Langmuir* **1997**, *13*, 2113.
(10) Manciu, M.; Ruckenstein, E. *Langmuir* **2001**, *17*, 7582.
(11) Berkowitz, M. L.; Raghavan, K. *Langmuir* **1991**, *7*, 1042.
(12) Essmann, U.; Perera, L.; Berkowitz, M. L. *Langmuir* **1995**, *11*, 4519.
(13) Perera, L.; Essmann, U.; Berkowitz, M. L. *Langmuir* **1996**, *12*, 2625.
(14) Pertsin, A.; Platonov, D.; Grunze, M. *J. Chem. Phys.* **2005**, *122*, 244708.
(15) Lu, L.; Berkowitz, M. L. *J. Chem. Phys.* **2006**, *124*, 101101.
(16) Pertsin, A.; Platonov, D.; Grunze, M. *Langmuir* **2007**, *23*, 1388.
(17) Eun, C.; Berkowitz, M. L. *J. Phys. Chem. B* **2009**, *113*, 13222.
(18) Berne, B. J.; Weeks, J. D.; Zhou, R. H. *Annu. Rev. Phys. Chem.* **2009**, *60*, 85.
(19) Chandler, D. *Nature* **2005**, *437*, 640.
(20) Lum, K.; Chandler, D.; Weeks, J. D. *J. Phys. Chem. B* **1999**, *103*, 4570.
(21) Choudhury, N.; Pettitt, B. M. *J. Am. Chem. Soc.* **2007**, *129*, 4847.
(22) Choudhury, N.; Pettitt, B. M. *J. Phys. Chem. B* **2006**, *110*, 8459.
(23) Choudhury, N.; Pettitt, B. M. *J. Am. Chem. Soc.* **2005**, *127*, 3556.
(24) Lu, L.; Berkowitz, M. L. *Mol. Phys.* **2006**, *104*, 3607.
(25) Nagle, J. F.; Tristram-Nagle, S. *Biochim. Biophys. Acta: Rev. Biomembr.* **2000**, *1469*, 159.
(26) Pandit, S. A.; Bostick, D.; Berkowitz, M. L. *Biophys. J.* **2003**, *84*, 3743.
(27) Tieleman, D. P.; Marrink, S. J.; Berendsen, H. J. C. *Biochim. Biophys. Acta: Rev. Biomembr.* **1997**, *1331*, 235.
(28) Berendsen, H. J. C.; Grigera, J. R.; Straatsma, T. P. *J. Phys. Chem.* **1987**, *91*, 6269.
(29) Nose, S. J. *J. Chem. Phys.* **1984**, *81*, 511.
(30) Hoover, W. G. *Phys. Rev. A* **1985**, *31*, 1695.
(31) Parrinello, M.; Rahman, A. *J. Appl. Phys.* **1981**, *52*, 7182.
(32) Essmann, U.; Perera, L.; Berkowitz, M. L.; Darden, T.; Lee, H.; Pedersen, L. G. *J. Chem. Phys.* **1995**, *103*, 8577.
(33) Iuchi, S.; Chen, H.; Paesani, F.; Voth, G. A. *J. Phys. Chem. B* **2009**, *113*, 4017.
(34) Jedlovszky, P.; Brodholt, J. P.; Bruni, F.; Ricci, M. A.; Soper, A. K.; Vallauri, R. *J. Chem. Phys.* **1998**, *108*, 8528.
(35) Hess, B. *J. Chem. Phys.* **2002**, *116*, 209.
(36) Lindahl, E.; Hess, B.; van der Spoel, D. *J. Mol. Model.* **2001**, 306.
(37) Zangi, R.; Berne, B. J. *J. Phys. Chem. B* **2008**, *112*, 8634.
(38) Bhide, S. Y.; Berkowitz, M. L. *J. Chem. Phys.* **2005**, *123*, 224702.
(39) Pal, S.; Balasubramanian, S.; Bagchi, B. *J. Phys. Chem. B* **2003**, *107*, 5194.
(40) Bruce, C. D.; Senapati, S.; Berkowitz, M. L.; Perera, L.; Forbes, M. D. E. *J. Phys. Chem. B* **2002**, *106*, 10902.
(41) Senapati, S.; Berkowitz, M. L. *J. Chem. Phys.* **2003**, *118*, 1937.
(42) Lee, S. H.; Rossky, P. J. *J. Chem. Phys.* **1994**, *100*, 3334.
(43) Kjellander, R.; Marcelja, S. *Chem. Phys. Lett.* **1985**, *120*, 393.

JP910347N